This paper is published as part of a *PCCP* themed issue on chemical dynamics of large amplitude motion

Guest editors: David J. Nesbitt and Martin A. Suhm

Editorial

Papers

High resolution electronic spectroscopy of 4-methylanisole in the gas phase. Barrier height determinations for the methyl group torsional motion
Philip J. Morgan, Leonardo Alvarez-Valtierra and David W. Pratt, *Phys. Chem. Chem. Phys*., 2010
DOI: 10.1039/c000757a

Determination of precise relative energies of conformers of *n*-propanol by rotational spectroscopy
Zbigniew Kisiel, Orest Dorosh, Atsuko Maeda, Ivan R. Medvedev, Frank C. De Lucia, Eric Herbst, Brian J. Drouin, John C. Pearson and Steven T. Shipman, *Phys. Chem. Chem. Phys*., 2010
DOI: 10.1039/c002156c

Microwave spectroscopy of the Ne–OH($^2\Pi_j$) complex and three-dimensional intermolecular potentials
Yoshihiro Sumiyoshi, Ippei Funahara, Kazuya Sato, Yasuhiro Ohshima and Yasuki Endo, *Phys. Chem. Chem. Phys*., 2010
DOI: 10.1039/c002193h

Rotational spectra of *o*-, *m*-, and *p*-cyanophenol and internal rotation of *p*-cyanophenol
Andrew R. Conrad, Nathan Z. Barefoot and Michael J. Tubergen, *Phys. Chem. Chem. Phys*., 2010
DOI: 10.1039/c001705a

Hydrogen exchange in formic acid dimer: tunnelling above the barrier
David Luckhaus, Phys. Chem. Chem. Phys., 2010
DOI: 10.1039/c001253j

Tunneling dynamics and spectroscopic parameters of monodeuterated hydronium, H_2DO^+, from a combined analysis of infrared and sub-millimeter spectra
Holger S. P. Müller, Feng Dong, David J. Nesbitt, Takashi Furuya and Shuji Saito, *Phys. Chem. Chem. Phys*., 2010
DOI: 10.1039/c002067b

On the efficiency of treating singularities in triatomic variational vibrational computations. The vibrational states of H+3 up to dissociation
Tamás Szidarovszky, Attila G. Császár and Gábor Czakó, *Phys. Chem. Chem. Phys*., 2010
DOI: 10.1039/c001124j

Theoretical rotation–torsion spectra of HSOH
Andrey Yachmenev, Sergei N. Yurchenko, Per Jensen, Oliver Baum, Thomas F. Giesen and Walter Thiel, *Phys. Chem. Chem. Phys*., 2010
DOI: 10.1039/c002803g

Chirality of and gear motion in isopropyl methyl sulfide: A Fourier transform microwave study
Eizi Hirota, Keisuke Sakieda and Yoshiyuki Kawashima, *Phys. Chem. Chem. Phys*., 2010
DOI: 10.1039/c002314k

Torsional energy levels of nitric acid in reduced and full dimensionality with ElVibRot and Tnum
David Lauvergnat and André Nauts, Phys. Chem. Chem. Phys., 2010
DOI: 10.1039/c001944e

Theoretical rotation–torsion spectra of HSOH†

Andrey Yachmenev,[a] Sergei N. Yurchenko,[b] Per Jensen,*[c] Oliver Baum,[d] Thomas F. Giesen[d] and Walter Thiel[a]

Received 9th February 2010, Accepted 17th May 2010
First published as an Advance Article on the web 5th June 2010
DOI: 10.1039/c002803g

Rotation–torsion spectra of HSOH, involving the vibrational ground state and the fundamental torsional state, have been simulated at $T = 300$ K. The simulations are carried out with the variational computer program TROVE in conjunction with recently reported *ab initio* potential energy and electric dipole moment surfaces. HSOH is a near-prolate-symmetric top at equilibrium and the simulated spectra are of perpendicular-band-type with strong *R*-branch and *Q*-branch transitions. Recently, an anomalous (*b*-type-transition)/(*c*-type-transition) intensity ratio in the vibrational-ground-state ${}^rQ_{K_a}$-branches of HSOH has been experimentally observed. Our calculations reproduce correctly the anomaly and show that it originates in the large-amplitude torsional motion of HSOH. We analyze our theoretical results in order to explain the effect and to provide unambiguous (*b*/*c*)-type-transition assignments.

I. Introduction

Sulfur compounds play important roles in biochemistry,[1] in atmospheric processes,[2–4] and in combustion chemistry.[5] In particular, there is evidence[2–4] that oxadisulfane HSOH is involved in the formation of pollutants in the upper layers of the terrestrial atmosphere. Consequently, the study of HSOH becomes a prerequisite for understanding atmospheric sulfur chemistry. In addition, HSOH is the first example of a skew-chain molecule with two different internal-rotor moieties (OH and SH) to be spectroscopically characterized at high resolution.[6–13] The rotation–vibration energies of HSOH exhibit splittings caused by the large-amplitude internal rotation of the OH and SH moieties about the OS bond. Already in the initial spectroscopic characterization of HSOH,[6] it became apparent that the variation of the splittings with rotational excitation was very different from, and much more complicated than, the splitting pattern previously observed for the related molecules HOOH and HSSH (see, for example, ref. 14 and the references therein). We have previously made theoretical analyses[14–17] of the HSOH splitting pattern, thus explaining the spectroscopic observations, and in the present work we extend the theoretical description of HSOH to the simulation of rotation–torsion spectra with the aim of explaining recently observed 'anomalous' intensities.[12] Since HSOH can be considered a prototype skew-chain molecule with two different internal rotors, we believe that the theoretical study of the torsional energy splittings reported in ref. 14–17, together with the intensity analyses of the present work, will assist future experimental investigations of molecules of this type.

In ref. 16, we have reported the *ab initio* potential energy and dipole moment surfaces for the electronic ground state of HSOH used in the present work. These surfaces were calculated by the CCSD(T) method (coupled-cluster theory with single and double excitations[18] and a perturbative treatment of triple excitations)[19] with the aug-cc-pV(T + *d*)Z and aug-cc-pV(Q + *d*)Z (augmented correlation-consistent triple- and quadruple-zeta) bases.[20–23] We used in ref. 16 the *ab initio* data and the program TROVE[24] to determine theoretical values for the fundamental vibrational band centers and the vibrational transition moments of HSOH. Prior to publication of the potential energy surface (PES), we had already applied it[15] for calculating with TROVE the rotation–torsion term values of HSOH for $J \leq 40$. As mentioned above, with the results of ref. 15 we could explain the initially unexpected variation of the torsional splittings with rotational excitation (ref. 14, 17).

The very recent ref. 12 reported accurate spectral data of $H^{32}SOH$ recorded at 1.3 THz. These spectra exhibited an unexpected effect in that for $H^{32}SOH$, no *b*-type transitions were observed in the ${}^rQ_3$-branch of the vibrational ground state. This effect was not explained in ref. 12 and the primary aim of the present paper is to provide an explanation. Towards this end, we simulate the rotation–torsion spectrum of $H^{32}SOH$ (henceforth referred to as HSOH) by means of the program suite TROVE. The term values and eigenfunctions needed for constructing the spectra are generated in the so-called *reaction path* Hamiltonian (RPH) approach[25] (also known as the *semirigid bender* (SRB) approach),[26,27] the TROVE version of which is based on the integration along the minimum energy path (MEP). We use the MEP of HSOH reported in ref. 15. We can explain the intensity anomaly observed for HSOH in terms of our theoretical results, and by analyzing the intensity results we can provide unambiguous (*b*/*c*)-type-transition assignments.

[a] *Max-Planck-Institut für Kohlenforschung, Kaiser-Wilhelm-Platz 1, D–45470 Mülheim an der Ruhr, Germany*
[b] *Technische Universität Dresden, Institut für Physikalische Chemie und Elektrochemie, D-01062 Dresden, Germany*
[c] *FB C – Theoretische Chemie, Bergische Universität, D–42097 Wuppertal, Germany. E-mail: jensen@uni-wuppertal.de*
[d] *I. Physikalisches Institut, Universität zu Köln, Zülpicher Straße 77, D-50937 Köln, Germany*

† Electronic supplementary information (ESI) available: Line lists for all transitions discussed in the paper. See DOI: 10.1039/c002803g

The paper is structured as follows. In section II the variational TROVE method is described. The theoretical rotation–torsion spectrum is presented and discussed in section III, where the intensity anomaly of the $^{r}Q_3$ branch is analyzed. In this section we also predict the fundamental and hot torsional bands. Some conclusions are presented in section IV.

II. Details of the TROVE calculation

For the calculation of the rotation–torsion energies of HSOH together with the eigenfunctions necessary for the intensity calculations we employ the variational method as implemented in the program TROVE.[24] In the calculations we use the computational setup applied in ref. 15 for the analysis of the torsional energy-level splittings of HSOH. Consequently, the reader is referred to ref. 15 for the details of the basis set, the Hamiltonian and the computational method. It suffices to say here that, as mentioned above, we employ the RPH/SRB approach[25–27] in which the rotation–vibration Hamiltonian is expanded around the torsional minimum energy path of HSOH.[15] The RPH/SRB calculations are based on the MEP from ref. 15 which, in turn, is obtained from the *ab initio* PES of ref. 16. In order to improve the agreement with experiment we have performed an empirical adjustment of the MEP from ref. 15 by adjusting the value of a_0^{OS} (the new value is 1.68712 Å), which defines the OS-bond length at the planar *trans* configuration of the molecule.

The basis set employed in the RPH/SRB calculations is identical to that of ref. 15. The basis functions are given by products

$$|\phi_{\mathrm{rv}}\rangle = |v_{\mathrm{OS}}\rangle|v_{\mathrm{SH}}\rangle|v_{\mathrm{OH}}\rangle|v_{\mathrm{OSH}}\rangle|v_{\mathrm{SOH}}\rangle|v_{\mathrm{HSOH}},\tau_{\mathrm{tor}}\rangle|J,\, K,\, \tau_{\mathrm{rot}}\rangle, \quad (1)$$

where v_{X} is the principal quantum number for the vibrational mode ν_{X} (X = OS, SH, OH, OSH, and SOH in an obvious notation; ν_{HSOH} is the torsional mode), $\tau_{\mathrm{tor}} = 0$ or 1 determines the torsional parity[28] as $(-1)^{\tau_{\mathrm{tor}}}$, and $\tau_{\mathrm{rot}} = 0$ or 1 determines the rotational parity[28] as $(-1)^{\tau_{\mathrm{rot}}}$. The total parity of the basis state $|\phi_{\mathrm{rv}}\rangle$ is consequently $(-1)^{\tau_{\mathrm{tor}}+\tau_{\mathrm{rot}}}$. We label the rotational states by quantum numbers $\{J, K, \tau_{\mathrm{rot}}\}$ that correlate with the customary ones J_{K_a,K_c} according to

$$K_a = K,\ K_c = J - K_a + \tau_{\mathrm{rot}}. \quad (2)$$

The one-dimensional small-amplitude vibrational basis functions $|v_{\mathrm{X}}\rangle$ and the torsional basis functions $|v_{\mathrm{HSOH}}, \tau_{\mathrm{tor}}\rangle$ are generated by means of the Numerov–Cooley method.[29]

In the RPH/SRB calculations, we follow ref. 15 in setting $v_{\mathrm{OS}} = v_{\mathrm{SH}} = v_{\mathrm{OH}} = v_{\mathrm{OSH}} = v_{\mathrm{SOH}} = 0$. Consequently, the rotation–torsion eigenfunctions $\Psi_{J,\Gamma,i}$ are obtained as the variational solution

$$\Psi_{J,\Gamma,i} = |0\rangle \sum_{v_{\mathrm{HSOH}},\tau_{\mathrm{tor}},K,\tau_{\mathrm{rot}}} C_{J,\Gamma,i}^{(K,\tau_{\mathrm{rot}},v_{\mathrm{HSOH}},\tau_{\mathrm{tor}})} |v_{\mathrm{HSOH}},\tau_{\mathrm{tor}}\rangle|J,K,\tau_{\mathrm{rot}}\rangle, \quad (3)$$

to the rotation–torsion Schrödinger equation. Here, the $C_{J,\Gamma,i}^{(K,\tau_{\mathrm{rot}},v_{\mathrm{HSOH}},\tau_{\mathrm{tor}})}$ are expansion coefficients and '$|0\rangle$' is a shorthand notation for $|0\rangle|0\rangle|0\rangle|0\rangle|0\rangle$ where each zero is the value of one of the vibrational quantum numbers v_{X}, X = OS, SH, OH, OSH, and SOH. We have introduced Γ (= A' or A'') to denote an irreducible representation of the molecular symmetry group C_s(M) (see Table A-2 of ref. 28) generated by the eigenfunction $\Psi_{J,\Gamma,i}$. The running index i labels eigenstates with the same values of J and Γ.

The approach to simulate absorption spectra implemented in TROVE is based on the theory described in detail in ref. 30. This theory was developed in connection with the program XY3,[31] a fore-runner program for TROVE, and the modifications related to the specifics of the TROVE program have been reported in ref. 32. The expression for the line strength $S(f \leftarrow i)$ is given in Appendix A. In all spectrum simulations, we have assumed the HSOH molecules to be in thermal equilibrium at an absolute temperature of $T = 300$ K. In order to reduce the computation time we have applied a pre-screening procedure to truncate the wavefunction expansions in eqn (3): All terms with $|C_{J,\Gamma,i}^{(K,\tau_{\mathrm{rot}},v_{\mathrm{HSOH}},\tau_{\mathrm{tor}})}|^2 < 10^{-14}$ are neglected in the computation of $S(f \leftarrow i)$.

In the present study we employ the HSOH dipole moment surface denoted as ACV(T + *d*) in ref. 16. We expand it as a Taylor series in the internal coordinates similar to the expansion of the potential energy function (see section 4 of ref. 24). The expansion coefficients are determined as partial derivatives of the *ab initio* dipole moment components. These components are evaluated numerically by the finite-difference method. The expansions of the dipole moment components are truncated after the fourth order terms.

The expression for the intensity of an absorption line for the transition from the state i with energy E_i, in thermal equilibrium at the temperature T, to the state f with energy E_f is given by ref. 28,

$$I(f \leftarrow i) = \int_{\mathrm{Line}} \epsilon(\tilde{\nu})\mathrm{d}\tilde{\nu} = \frac{8\pi^3 N_{\mathrm{A}} \tilde{\nu}_{if}}{(4\pi\varepsilon_0)3hc} \frac{e^{-E_i/kT}}{Q}[1 - \exp(-hc\tilde{\nu}_{if}/kT)]S(f \leftarrow i), \quad (4)$$

where $hc\tilde{\nu}_{if} = E_f - E_i$, N_{A} is the Avogadro constant, h is Planck's constant, c is the speed of light in vacuum, k is the Boltzmann constant, ε_0 is the permittivity of free space, and $S(f \leftarrow i)$ is the line strength defined in eqn (26) of Appendix A. The partition function Q is given by

$$Q = \sum_j g_j \mathrm{e}^{-E_j/kT}, \quad (5)$$

where g_j is the total degeneracy of the state with energy E_j and the sum runs over all energy levels of the molecule. Because of the constraints in the specification of the RPH/SRB basis set [eqn (3)], we cannot proceed in the usual manner and evaluate Q in eqn (5) by summing over all energy levels obtained in the TROVE variational calculation; the levels with excited quanta of the small-amplitude vibrational modes ν_{X} (X = OS, SH, OH, OSH, and SOH) would then be missing from the sum. In order to circumvent this problem we employ the theoretical vibrational term values from ref. 16 and approximate $Q \approx Q_{\mathrm{vib}} \times Q_{\mathrm{rot}}$, where Q_{vib} and Q_{rot} are vibrational and rotational partition functions, respectively. This approximation for Q is equivalent to the neglect of rotation–vibration

interaction. The rotational partition function Q_{rot} is taken to have the rigid-rotor value[33]

$$Q_{rot} = g_{ns}\frac{\sqrt{\pi}}{\sigma\sqrt{ABC}}\left(\frac{kT}{hc}\right)^{3/2}, \qquad (6)$$

where the symmetry number $\sigma = 1$ for HSOH and the values of the rotational constants A, B, and C are from ref. 12. In eqn (6), we have included the effect of nuclear spin degeneracies through the nuclear spin statistical weight factor g_{ns} ($g_{ns} = 4$ for all rovibrational states of HSOH). For $T = 300$ K we obtain $Q_{rot} = 16368.12$. The vibrational partition function Q_{vib} is computed from the vibrational term values of ref. 16 with the summation limited to vibrational levels below 10 000 cm^{-1}. We obtain $Q_{vib} = 2.37$ and so the total partition function for HSOH, $Q = Q_{vib} \times Q_{rot} = 38792.48$ at $T = 300$ K. The approximation $Q = Q_{vib} \times Q_{rot}$ is probably not highly accurate but we expect that it produces a Q value of the correct order of magnitude. It should be emphasized that a more accurate Q value would not alter any of the conclusions drawn in the present work. We discuss here relative intensities which are not dependent on the value of Q. A change of the Q value employed in the calculations has the effect of multiplying all computed intensities by a common factor [eqn (4)].

III. The theoretical rotation–torsion absorption spectrum of HSOH at $T = 300$ K

Fig. 1 shows the $J \leq 40$ simulated rotational spectrum (in the vibrational ground state) of HSOH below 180 cm^{-1}. Owing to the torsional tunneling between two minima on the potential energy surface, each transition is split into a doublet.[14,17] Line lists for the transitions in the Figure and for all transitions discussed in the remainder of the paper are available as ESI.† In the stick diagram of Fig. 1, the height of a stick represents the integrated absorption coefficient computed from eqn (4). When the wavenumbers of two or more transitions coincide, the intensities of these transitions are added to give the height of the stick. The most prominent features of the spectrum in the figure are the wide $^rR_{K_a}$ branches whose transitions are drawn as grey sticks. These branches start abruptly on the low-wavenumber side with the transition $J = K_a+1 \leftarrow K_a$; the other transitions in a given branch correspond to higher J values and fall at higher wavenumber values. The narrow $^rQ_{K_a}$ branches are marked by asterisks, and the $^rP_{K_a}$ branches (marked by arrows) are comparatively weak.

Each low-lying rovibrational energy level of HSOH is split into two torsional components of symmetry A' or A'', respectively, in the molecular symmetry group $\boldsymbol{C}_s$(M). This fact, in conjunction with the electric-dipole-transition selection rule[28] of $A' \leftrightarrow A''$ (or, equivalently, $|\Delta(\tau_{tor} + \tau_{rot})| = 1$), causes each rotational transition to split into a doublet (see also ref. 15).

Along the entire torsional MEP of HSOH, the dipole moment is almost perpendicular to the SO bond. The principal axis of least moment of inertia a is approximately parallel to the SO bond and so HSOH has a relatively small 'parallel' dipole moment component $\bar{\mu}_a$, (see Fig. 2 in ref. 16) and large 'perpendicular' components $\bar{\mu}_b$ and $\bar{\mu}_c$. Since we associate the a axis with the molecule-fixed z axis[28] for the near-prolate-symmetric top HSOH, the strong transitions in the rotational spectrum have $|\Delta K_a| \neq 0$ as shown in Fig. 1 (see also ref. 12). Customarily, these strong transitions are further classified as being of b-type (c-type) if their intensity originates predominantly in the dipole moment component $\bar{\mu}_b$ ($\bar{\mu}_c$). A b-type transition has $\Delta\tau_{tor} = 0$ (and $|\Delta\tau_{rot}| > 0$) because $\bar{\mu}_b$ has A' symmetry in $\boldsymbol{C}_s$(M). Conversely, a c-type transition has $|\Delta\tau_{tor}| > 0$ (and $\Delta\tau_{rot} = 0$) because $\bar{\mu}_c$ has A'' symmetry. This normally allows observed lines to be identified according to their intensities: In the first approximation the ratio between the intensities of the b- and c-type transitions is roughly equal to the ratio between the squares of $\bar{\mu}_b$ and $\bar{\mu}_c$:

$$\frac{I_b}{I_c} \approx \frac{\bar{\mu}_b^2}{\bar{\mu}_c^2}. \qquad (7)$$

If this relation is satisfied, the structures of the observed spectrum can be recognized as being of b-type or c-type. This effect is general for (semi-)rigid symmetric tops[28,34] with a small $\bar{\mu}_a$-value and has been observed in HSOH spectra.[6]

From the equilibrium values of the HSOH *ab initio* dipole moment components,[16] $\bar{\mu}_b^{eq} = 0.744$ D and $\bar{\mu}_c^{eq} = 1.399$ D, we obtain from eqn (7) $I_b/I_c \approx 0.28$. The corresponding vibrationally averaged values for the vibrational ground state are $\bar{\mu}_b^{eq} = 0.699$ D and $\bar{\mu}_c^{eq} = 1.297$ D;[16] these values produce $I_b/I_c \approx 0.29$. The experimentally derived intensity ratio for the $^rQ_0$ and $^rQ_1$ branches of the HSOH rotational spectrum has been reported to be very close to this value; $I_b/I_c \approx 0.22(4)$ for the $^rQ_0$ branch and 0.23(2) for $^rQ_1$ where the quantities in parentheses are quoted uncertainties in units of the last decimal given (see also ref. 12). For the $^rQ_2$ and $^rQ_3$ branches, however, eqn (7) is not satisfied: I_b/I_c is experimentally determined to be 0.58(11) for the $^rQ_2$ branch, and for the $^rQ_3$ branch the ratio was found to be below 0.02. In ref. 12, this 'intensity anomaly' was attributed to mixing of basis states. It is illustrated in Fig. 2 which shows the $^rQ_2$ and $^rQ_3$ branches from ref. 12. The $^rQ_2$ branch has been recorded with the Cologne THz spectrometer[35] whereas for the $^rQ_3$ branch measurements at 1.3 THz, a synthesizer-based multiplier spectrometer was employed. In this Figure, the assigned transitions of the stick

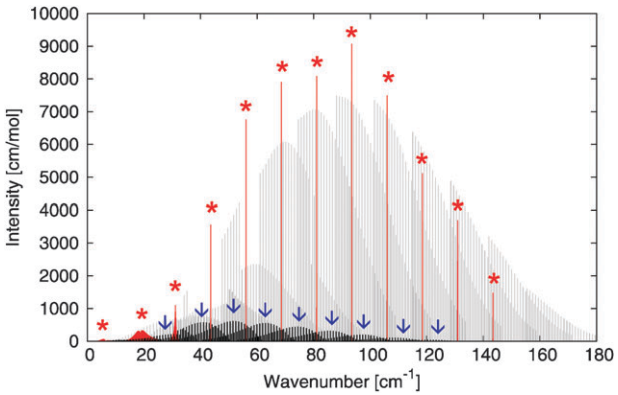

Fig. 1 Simulated rotational spectrum of HSOH at $T = 300$ K. All prominent transitions have $\Delta K_a = 1$. The ^rP and ^rQ branches are indicated by arrows and asterisks, respectively. The strongest transitions are found in the ^rR-branches.

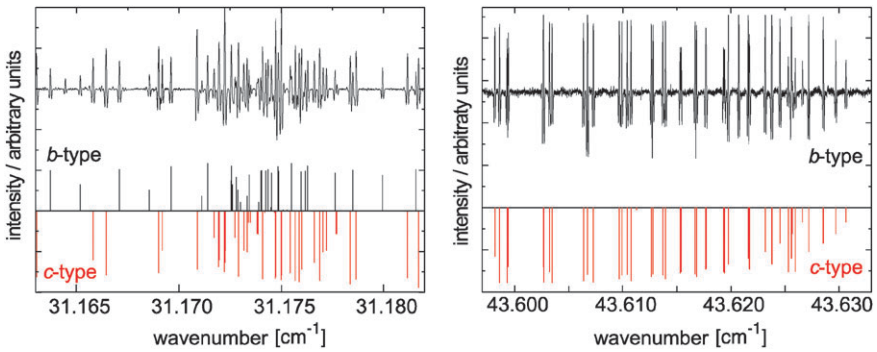

Fig. 2 Band heads of the ${}^{r}Q_2$ and ${}^{r}Q_3$ branches[12] of HSOH in the vibrational ground state. Below the experimental spectra, the assignments to *b*-type and *c*-type transitions are indicated by stick spectra drawn in black and red, respectively.

spectrum are colour-coded: *c*-type transitions are drawn in red and *b*-type transitions are drawn in black.

In Fig. 3, we plot simulated stick spectra of the ${}^{r}Q_{K_a}$ (K_a = 0, 1, 2, 3) branches in the vibrational-ground-state rotational spectrum of HSOH. The colour-coding is the same as in Fig. 2 and the *b*-type transitions are drawn upside-down so as to distinguish them better from the *c*-type transitions. The ${}^{r}Q_0$, ${}^{r}Q_1$, and ${}^{r}Q_2$ branches all have an appreciable number of both *b*-type and *c*-type transitions with an intensity ratio $I_b/I_c \approx 1/3$ in agreement with eqn (7). However, in agreement with the experimental findings, the ${}^{r}Q_3$ branch hardly has *b*-type transitions at all.

In order to understand the intensity anomaly of the ${}^{r}Q_{K_a}$ branches we analyze the eigenfunctions in eqn (3) for the rotation–torsion states involved. Recently[15] we have shown that the rotational quantum number K_a for HSOH is a nearly-good quantum number even for high J. This is in agreement with the experimental observations[6] and typical for this type of molecule (*e.g.*, HOOH[36] and HSSH[37]). Therefore we can safely use K_a to assign the rotational states being analyzed. Each rotation–torsion state characterized by the quantum numbers J, K_a is torsionally and rotationally split into four components (see Fig. 4). These states span the representation $2A' \oplus 2A''$ of $\boldsymbol{C}_s$(M) and, in consequence, the corresponding eigenfunctions can be denoted as $\Psi^{A',(1)}_{J,K_a,i}$, $\Psi^{A',(2)}_{J,K_a,i}$, $\Psi^{A'',(1)}_{J,K_a,i}$, and $\Psi^{A'',(2)}_{J,K_a,i}$, where the index i determines the torsional excitation. For the states considered, the torsional splitting varies in the range 0.0005–0.00025 cm^{-1} and shows a strong dependence on K_a.[12,15] The rotational (asymmetry) splitting for the asymmetric (but near-prolate-symmetric) top HSOH is apparent only for low K_a[34] and cannot be resolved experimentally at $K_a \geq 4$[12,15] (see the top-right display of Fig. 4). Analyzing the expansion coefficients of eqn (3) we find that in a good approximation, the four eigenfunctions associated with given values of J, K_a ($K_a > 0$) can be modeled by the expressions

$$\Psi^{A',(1)}_{J,K_a,i} \approx c_{J,K_a}|J,K_a,0\rangle\phi^{(\mathrm{vib})}_{K_a,0} + s_{J,K_a}|J,K_a,1\rangle\phi^{(\mathrm{vib})}_{K_a,1}, \quad (8)$$

$$\Psi^{A',(2)}_{J,K_a,i} \approx -s_{J,K_a}|J,K_a,0\rangle\phi^{(\mathrm{vib})}_{K_a,0} + c_{J,K_a}|J,K_a,1\rangle\phi^{(\mathrm{vib})}_{K_a,1}, \quad (9)$$

$$\Psi^{A'',(1)}_{J,K_a,i} \approx c_{J,K_a}|J,K_a,0\rangle\phi^{(\mathrm{vib})}_{K_a,1} + s_{J,K_a}|J,K_a,1\rangle\phi^{(\mathrm{vib})}_{K_a,0}, \quad (10)$$

$$\Psi^{A'',(2)}_{J,K_a,i} \approx -s_{J,K_a}|J,K_a,0\rangle\phi^{(\mathrm{vib})}_{K_a,1} + c_{J,K_a}|J,K_a,1\rangle\phi^{(\mathrm{vib})}_{K_a,0}, \quad (11)$$

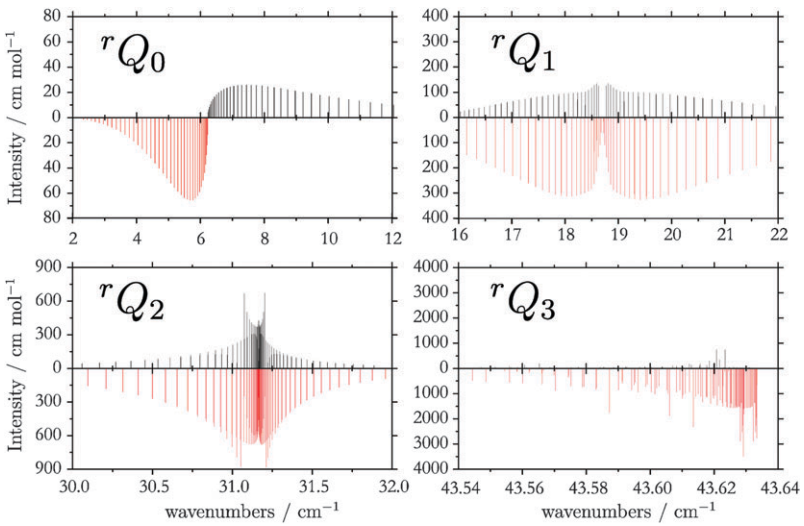

Fig. 3 ${}^{r}Q_{K_a}$ (K_a = 0, 1, 2, 3) branches in the rotational spectrum of HSOH, simulated at an absolute temperature of T = 300 K. Transitions assigned as *b*-type transitions are drawn in black, and *c*-type transitions are drawn upside-down in red. The *b*/*c*-type assignment is made by comparing the $|T^{\mathrm{if}}_b|$ and $|T^{\mathrm{if}}_c|$ contributions in eqn (25) (see text).

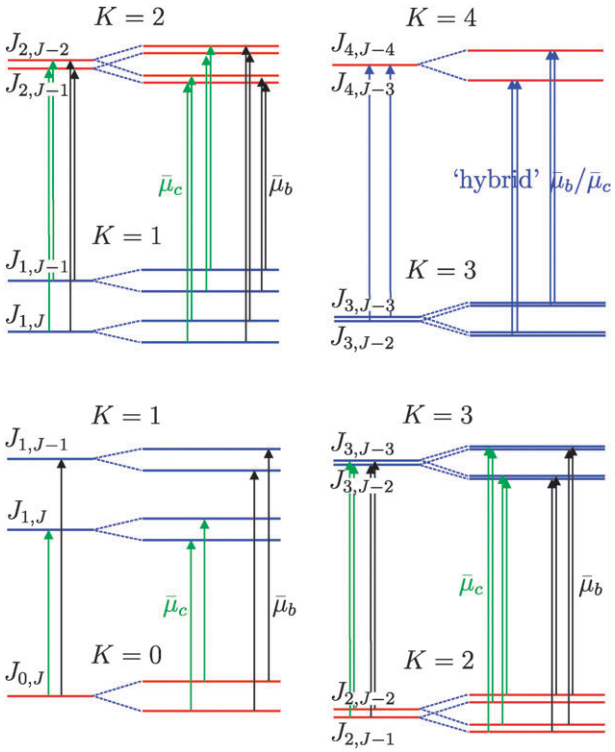

Fig. 4 Term level diagram showing the ${}^{r}Q_{K_a}$ ($K_a \leq 3$) transitions of HSOH. The 'experimental' quantum numbers are indicated as given by eqn (2).

where $c_{J,K_a} = \cos(\theta_{J,K_a})$ and $s_{J,K_a} = \sin(\theta_{J,K_a})$ with the mixing angle $\theta_{J,K_a} \in [0, \pi/4]$ so that $c_{J,K_a} \geq s_{J,K_a}$. Further, in eqn (8)–(11)

$$\phi^{(\mathrm{vib})}_{K_a,\tau_{\mathrm{tor}}} \approx |0\rangle \sum_{v_{\mathrm{HSOH}}} C^{(K_a,\tau_{\mathrm{rot}},v_{\mathrm{HSOH}},\tau_{\mathrm{tor}})}_{J,\Gamma,i} |v_{\mathrm{HSOH}},\tau_{\mathrm{tor}}\rangle, \qquad (12)$$

where the expansion coefficients $C^{(K_a,\tau_{\mathrm{rot}},v_{\mathrm{HSOH}},\tau_{\mathrm{tor}})}_{J,\Gamma,i}$ are defined in eqn (3). Our previous analyses of the torsion–rotation wavefunctions[15] suggest, together with our experience with semi-empirical models[14,17] for explaining the rotation–torsion splittings in HSOH, that as indicated in eqn (12) (the right hand side can be evaluated for any τ_{rot}-value available) the vibrational basis functions $\phi^{(\mathrm{vib})}_{K_a,\tau_{\mathrm{tor}}}$ are largely independent of τ_{rot}.

We aim at calculating the line strengths for the ${}^{r}Q_{K_a}$ transitions originating in one four-member manifold of states with wavefunctions defined by eqn (8)–(11) and ending in another such manifold. In principle, there are 16 possible transitions but owing to the symmetry selection rule $\Gamma = A' \leftrightarrow A''$ only eight of these have a nonvanishing intensity.

We now insert eqn (8)–(11) in the general expression for the line strength $S(f \leftarrow i)$ (see Appendix A) to obtain the desired line strengths. We employ the fact that because of symmetry, non-vanishing vibrational matrix elements of $\bar{\mu}_b$ are diagonal in τ_{tor} while non-vanishing vibrational matrix elements of $\bar{\mu}_c$ are off-diagonal in τ_{tor}. It is known from experience that vibrational dipole-moment matrix elements involving symmetrized vibrational basis functions normally depend weakly on parity labels, and so we initially assume that the non-vanishing vibrational matrix elements of the dipole moment components are independent of τ_{tor}:

$$\langle \phi^{(\mathrm{vib})}_{K_a,0} | \bar{\mu}_b | \phi^{(\mathrm{vib})}_{K_a+1,0} \rangle = \langle \phi^{(\mathrm{vib})}_{K_a,1} | \bar{\mu}_b | \phi^{(\mathrm{vib})}_{K_a+1,1} \rangle \qquad (13)$$

and

$$\langle \phi^{(\mathrm{vib})}_{K_a,0} | \bar{\mu}_c | \phi^{(\mathrm{vib})}_{K_a+1,1} \rangle = \langle \phi^{(\mathrm{vib})}_{K_a,1} | \bar{\mu}_c | \phi^{(\mathrm{vib})}_{K_a+1,0} \rangle. \qquad (14)$$

With these simplifications, we obtain for the eight non-vanishing transitions for a given J value in an ${}^{r}Q_{K_a}$ branch:

$$\begin{aligned} S_{A'(1)\leftrightarrow A''(1)} = S_{A'(2)\leftrightarrow A''(2)} &= g_{\mathrm{ns}} A(J,K_a) \\ &\times [\cos^2(\theta_{J,K_a+1} - \theta_{J,K_a}) \langle \phi^{(\mathrm{vib})}_{K_a,0} | \bar{\mu}_b | \phi^{(\mathrm{vib})}_{K_a+1,0} \rangle^2 \\ &+ \sin^2(\theta_{J,K_a+1} + \theta_{J,K_a}) \langle \phi^{(\mathrm{vib})}_{K_a,0} | \bar{\mu}_c | \phi^{(\mathrm{vib})}_{K_a+1,1} \rangle^2] \end{aligned} \qquad (15)$$

and

$$\begin{aligned} S_{A'(1)\leftrightarrow A''(2)} = S_{A'(2)\leftrightarrow A''(1)} &= g_{\mathrm{ns}} A(J,K_a) \\ &\times [\cos^2(\theta_{J,K_a+1} + \theta_{J,K_a}) \langle \phi^{(\mathrm{vib})}_{K_a,0} | \bar{\mu}_c | \phi^{(\mathrm{vib})}_{K_a+1,1} \rangle^2 \\ &+ \sin^2(\theta_{J,K_a+1} - \theta_{J,K_a}) \langle \phi^{(\mathrm{vib})}_{K_a,0} | \bar{\mu}_b | \phi^{(\mathrm{vib})}_{K_a+1,0} \rangle^2]. \end{aligned} \qquad (16)$$

Each symbol $S_{\Gamma_1(i_1)\leftrightarrow\Gamma_2(i_2)}$ in eqn (15) and (16) represents the line strength of two transitions, $\Gamma_1(i_1) \leftarrow \Gamma_2(i_2)$ and $\Gamma_2(i_2) \leftarrow \Gamma_1(i_1)$. $A(J, K_a)$ is a Hönl–London-type factor (see, for example, Chapter 12 of ref. 38) common to all ${}^{r}Q_{K_a}$ transitions with given values of J and K_a.

For $K_a = 0$, there is only one rotational basis function $|J, 0, \tau_{\mathrm{rot}}\rangle$ with $\tau_{\mathrm{rot}} = J \bmod 2$, and thus the two corresponding torsion–rotation eigenfunctions are defined by:

$$\Psi^{A'(1)}_{J,K_a=0,i} \approx |J,0,0\rangle \phi^{(\mathrm{vib})}_{K_a,0}, \qquad (17)$$

$$\Psi^{A''(1)}_{J,K_a=0,i} \approx |J,0,0\rangle \phi^{(\mathrm{vib})}_{K_a,1} \qquad (18)$$

for J even and

$$\Psi^{A'(2)}_{J,K_a=0,i} \approx |J,0,1\rangle \phi^{(\mathrm{vib})}_{K_a,1}, \qquad (19)$$

$$\Psi^{A''(2)}_{J,K_a=0,i} \approx |J,0,1\rangle \phi^{(\mathrm{vib})}_{K_a,0} \qquad (20)$$

for J odd. In applying eqn (15) and (16) to ${}^{r}Q_0$ transitions we can set $\theta_{J,0} = 0$.

Furthermore, for small $K_a > 0$ (in practice, $K_a = 1,2$) analyses of the TROVE calculations show that $\theta_{J,K_a} \approx 0$. For example, with $(J, K_a) = (10, 1)$ we have $c^2_{J,K_a} = 0.95$ and $s^2_{J,K_a} = 0.05$ corresponding to $\theta_{J,K_a} \approx 0.23$ rad (or 13°). That is, for $K_a = 0, 1, 2$ we can approximate $\theta_{J,K_a} = 0$ and so for the ${}^{r}Q_0$ and ${}^{r}Q_1$ transitions, $\theta_{J,K_a} = \theta_{J,K_a+1} = 0$ in eqn (15) and (16). These equations then simplify to

$$\begin{aligned} S_{A'(1)\leftrightarrow A''(1)} &= S_{A'(2)\leftrightarrow A''(2)} \\ &= g_{\mathrm{ns}} A(J,K_a) \langle \phi^{(\mathrm{vib})}_{K_a,0} | \bar{\mu}_b | \phi^{(\mathrm{vib})}_{K_a+1,0} \rangle^2 \end{aligned} \qquad (21)$$

and

$$\begin{aligned} S_{A'(1)\leftrightarrow A''(2)} &= S_{A'(2)\leftrightarrow A''(1)} \\ &= g_{\mathrm{ns}} A(J,K_a) \langle \phi^{(\mathrm{vib})}_{K_a,0} | \bar{\mu}_c | \phi^{(\mathrm{vib})}_{K_a+1,1} \rangle^2 \end{aligned} \qquad (22)$$

and the resulting relations are consistent with eqn (7). Eqn (21) defines a *b*-type transition, while eqn (22) defines a *c*-type transition. Obviously, the simplified theory presented here explains the experimentally derived intensity ratios of $I_b/I_c \approx 0.22$ for the $^rQ_0$ branch and 0.23 for $^rQ_1$ (ref. 12).

In ref. 15 we found that at higher K_a-values, the rotation–torsion wavefunctions become equal mixtures of the $|J, K_a, \tau_{\rm rot} = 0\rangle$ and $|J, K_a, \tau_{\rm rot} = 1\rangle$ basis functions (see Fig. 8 of ref. 15 and the associated discussion). For example, for $J = 10$, $K_a = 5$ the TROVE calculation yields $c^2_{J,K_a} = 0.48$ and $s^2_{J,K_a} = 0.52$ [eqn (8)–(11)], corresponding to $\theta_{J,K_a} \approx 0.81$ rad (or 46°). We have $\lim_{K_a\to\infty}\theta_{J,K_a} = \pi/4$ (or 45°). In this limit, eqn (15) and (16) simplify to

$$S_{A'(1)\leftrightarrow A''(1)} = S_{A'(2)\leftrightarrow A''(2)} = g_{\rm ns}A(J,K_a)[\langle\phi^{(\rm vib)}_{K_a,0}|\bar{\mu}_b|\phi^{(\rm vib)}_{K_a+1,0}\rangle^2 + \langle\phi^{(\rm vib)}_{K_a,0}|\bar{\mu}_c|\phi^{(\rm vib)}_{K_a+1,1}\rangle^2]$$

and

$$S_{A'(1)\leftrightarrow A''(2)} = S_{A'(2)\leftrightarrow A''(1)} = 0. \qquad (24)$$

It is obviously meaningless to assign transitions as being *b*-type or *c*-type in this situation, but we see that for large K_a, we obtain half as many $^rQ_{K_a}$ transitions as for, say, $K_a = 1$. This is consistent with the fact that for the $^rQ_3$ branch I_b/I_c is experimentally determined[12] to be below 0.02.

Fig. 5 shows values of $\theta_{J,K_a} = \arccos c_{J,K_a}$ computed from TROVE values of c_{J,K_a} for different values of K_a and $J = 10$. It is evident that the limiting value of $\lim_{K_a\to\infty}\theta_{J,K_a} = \pi/4$ (or 45°) is reached rather slowly as K_a increases. For the $^rQ_2$ branch, I_b/I_c is experimentally determined[12] to be 0.58. This value corresponds neither to the low-K_a limit of $\theta_{J,K_a} = \theta_{J,K_{a+1}} = 0$ nor to the high-K_a limit of $\theta_{J,K_a} = \theta_{J,K_{a+1}} = \pi/4$. The value of $\theta_{J,3} \approx 38°$ (Fig. 5) is intermediate between 0 and 45°.

To illustrate in greater detail how the intensities of the $^rQ_{K_a}$ transitions vary with K_a for HSOH, we collect in Table 1 information about these transitions for $J = 8$. We include in the Table the initial and final term values E_i and E_f, respectively, the transition wavenumbers ν_{if}, and absorption intensities $I(f \leftarrow i)$ [eqn (4)]. As discussed above in terms of the basis functions, for $K_a = 0$ there are two non-degenerate eigenstates, shown in Table 1 to be separated by 0.0022 cm^{-1}.

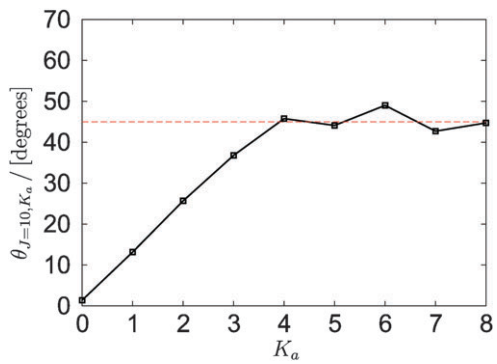

Fig. 5 Values of the angle $\theta_{J,K_a} = \arccos c_{J,K_a}$ [see eqn (8)–(11)] for different values of K_a and $J = 10$. The limiting value of $\theta_{J,K_a} = 45°$ is indicated by a horizontal dashed line.

For $K_a > 0$ there are always four eigenstates and when $K_a = 1$ or $K_a = 2$, these are all non-degenerate to an extent that with the four decimal places given in Table 1, four different energies ensue. For $K_a \geq 3$ the rotational (asymmetry) splittings become so small (see Table 3 of ref. 15 and the associated discussion) that the four eigenstates appear as two energy doublets (where, for each doublet, the member energies are equal to at least four decimal places). This is the *symmetric top limit* described in Fig. 9 of ref. 14. In Table 1, only two energies are given in these cases, and the effect of the double degeneracy on the transition intensities is indicated by a factor of ×2 [whilst non-degeneracy is indicated by a factor of ×1]. Owing to the general symmetry selection rule of $\Gamma = A' \leftrightarrow A''$, each J value gives rise to four $^rQ_{K_a} = 0$ transitions, eight $^rQ_{K_a} = 1$ transitions, eight $^rQ_{K_a} = 2$ transitions, and four resolved $^rQ_{K_a} \geq 3$ transitions as seen in Table 1.

Table 1 shows that for $J = 8$ (and also for all other J values) in the $^rQ_{K_a} = 0$ branch, there are two 'doublet' transitions, the members of each doublet being closely spaced (display $^rQ_0$ of Fig. 4). When, for $J = 8$, we take $I^{(b)}(f \leftarrow i)$ to be the sum of the intensities of the two doublet lines near 6.50 cm^{-1} and $I^{(c)}(f \leftarrow i)$ to be the sum of the intensities of the two doublet lines near 5.97 cm^{-1}, we have $I^{(b)}(f \leftarrow i)/I^{(c)}(f \leftarrow i) \approx 0.3 \approx I_b/I_c$ from eqn (7). Obviously, the two transitions near 6.50 cm^{-1} are *b*-type transitions while those near 5.97 cm^{-1} are *c*-type transitions.

The structure of the $^rQ_1$ branch is less apparent, but clearly we can separate the eight transitions (display $^rQ_1$ of Fig. 4) for $J = 8$ into a set of four 'weak' transitions (with $I(f \leftarrow i) < 110$ cm mol^{-1}) and a set of four 'strong' transitions (with $I(f \leftarrow i) > 210$ cm mol^{-1}). When we take $I^{(b)}(f \leftarrow i)$ to be the sum of the intensities of the four weak transitions and $I^{(c)}(f \leftarrow i)$ to be the sum of the intensities of the four strong transitions, we have again $I^{(b)}(f \leftarrow i)/I^{(c)}(f \leftarrow i) \approx 0.3 \approx I_b/I_c$ from eqn (7). Here, it is evident that the four weak transitions are of the *b*-type while the four strong transitions are of the *c*-type.

To investigate the $^rQ_{K_a}$ branches with $K_a \geq 2$ (see for example displays $^rQ_2$ and $^rQ_3$ of Fig. 4) we have found it instructive to analyze the TROVE values for the line strength $S(f \leftarrow i)$, calculated from the general expression in eqn (A1), in terms of the contributions from $\bar{\mu}_a$, $\bar{\mu}_b$, and $\bar{\mu}_c$:

$$S(f \leftarrow i) = g_{\rm ns}(2J+1)^2|T^{(\rm if)}(\bar{\mu}_a) + T^{(\rm if)}(\bar{\mu}_b) + T^{(\rm if)}(\bar{\mu}_c)|^2, \qquad (25)$$

where $J = J'' = J'$ and $T^{(\rm if)}(\bar{\mu}_\alpha)$ ($\alpha = a, b, c$) represent terms in the expression for $S(f \leftarrow i)$ involving the $\bar{\mu}_\alpha$ component only. The contributions $T^{(\rm if)}_b = T^{(\rm if)}(\bar{\mu}_b)$ and $T^{(\rm if)}_c = T^{(\rm if)}(\bar{\mu}_c)$ are included in Table 1; the corresponding $T^{(\rm if)}_a$ values are all found to be negligibly small. Now we can assign a transition as the *b*-type if $|T^{\rm if}_b| > |T^{\rm if}_c|$ in Table 1 and as the *c*-type if $|T^{\rm if}_c| > |T^{\rm if}_b|$. We immediately find that our *b*-type/*c*-type assignment of the $^rQ_0$ and $^rQ_1$ transitions is correct. We also find that it would be incorrect to base the assignment of $^rQ_2$ transitions on the individual transition intensities only: not all *b*-type transitions are weaker than all *c*-type transitions. When we now take $I^{(b)}(f \leftarrow i)$ to be the sum of the $I(f \leftarrow i)$ values for all $^rQ_2$ transitions, with $|T^{\rm if}_b| > |T^{\rm if}_c|$ and $I^{(c)}(f \leftarrow i)$ to be the analogous sum for all transitions with $|T^{\rm if}_c| > |T^{\rm if}_b|$, we obtain

Table 1 Initial and final term values E_i and E_f (in cm^{-1}), transition wavenumbers ν_{if} (in cm^{-1}), $\bar{\mu}_\alpha$-contribution T_α^{if} (in D, $\alpha = b, c$) to the line strength, and intensities $I(i \leftarrow f)$ (in cm mol^{-1}) for $J = 8$ transitions in the ${}^rQ_{K_a}$ branches of the HSOH rotational spectrum in the vibrational ground state. For each ${}^rQ_{K_a}$ branch, the theoretical value of the intensity ratio I_b/I_c is given (see text)

Branch	Γ_i	E_i	E_f	ν_{if}	T_b^{if}	T_c^{if}	$I(i \leftarrow f)$	I_b/I_c
${}^rQ_0$	A''	36.1484	42.1182	5.9698	0.021	0.217	59.0 × 1	
	A'	36.1462	42.1195	5.9732	−0.021	−0.217	58.9 × 1	
	A''	36.1484	42.6510	6.5026	0.119	0.003	18.1 × 1	
	A'	36.1462	42.6497	6.5035	−0.119	−0.003	18.3 × 1	0.3
${}^rQ_1$	A'	42.6510	61.0845	18.4335	0.028	0.149	291.7 × 1	
	A''	42.6497	61.0838	18.4341	0.004	0.149	216.7 × 1	
	A'	42.6510	61.0897	18.4387	0.081	−0.022	33.1 × 1	
	A''	42.6497	61.0903	18.4406	0.086	0.022	108.1 × 1	
	A''	42.1195	61.0838	18.9643	0.084	0.021	109.7 × 1	
	A'	42.1182	61.0845	18.9662	0.080	−0.021	33.6 × 1	
	A''	42.1195	61.0903	18.9708	−0.004	−0.146	220.2 × 1	
	A'	42.1182	61.0897	18.9715	−0.028	−0.146	296.4 × 1	0.3
${}^rQ_2$	A'	61.0903	92.2501	31.1598	0.013	0.145	589.1 × 1	
	A''	61.0897	92.2501	31.1604	0.082	0.046	388.3 × 1	
	A'	61.0903	92.2522	31.1619	−0.082	−0.005	175.1 × 1	
	A''	61.0897	92.2522	31.1625	0.011	−0.137	375.9 × 1	
	A''	61.0845	92.2501	31.1656	0.011	−0.137	376.0 × 1	
	A'	61.0838	92.2501	31.1663	0.082	0.005	175.1 × 1	
	A''	61.0845	92.2522	31.1677	−0.082	−0.046	388.4 × 1	
	A'	61.0838	92.2522	31.1684	0.013	0.145	589.4 × 1	0.6
${}^rQ_3$	A''	92.2522	135.8812	43.6290	0.042	0.129	1132.0 × 2	
	A''	92.2522	135.8832	43.6309	−0.066	0.051	8.5 × 2	
	A'	92.2501	135.8812	43.6311	0.066	−0.052	8.1 × 2	
	A'	92.2501	135.8832	43.6331	0.043	0.128	1132.6 × 2	0.007
${}^rQ_4$	A'	135.8832	191.9786	56.0955	0.048	0.112	1284.1 × 2	
	A'	135.8832	191.9804	56.0972	0.055	−0.065	4.5 × 2	
	A''	135.8812	191.9786	56.0974	−0.055	0.065	4.5 × 2	
	A''	135.8812	191.9804	56.0992	0.048	0.112	1284.3 × 2	0.003
${}^rQ_5$	A'	191.9804	260.5419	68.5616	−0.040	−0.103	1155.0 × 2	
	A''	191.9786	260.5419	68.5633	−0.052	0.052	0.0 × 2	
	A'	191.9804	260.5440	68.5636	0.052	−0.052	0.0 × 2	
	A''	191.9786	260.5440	68.5654	−0.040	−0.103	1155.2 × 2	1.2×10^{-6}
${}^rQ_6$	A''	260.5440	341.5716	81.0276	0.030	0.091	799.7 × 2	
	A''	260.5419	341.5716	81.0296	−0.047	0.036	6.9 × 2	
	A'	260.5440	341.5736	81.0296	−0.047	0.036	6.9 × 2	
	A'	260.5419	341.5736	81.0317	−0.030	−0.091	799.8 × 2	0.009

$I^{(b)}(f \leftarrow i)/I^{(c)}(f \leftarrow i) \approx 0.6$, in perfect agreement with the experimental value[12] of 0.58.

By comparing $|T_b^{if}|$ and $|T_c^{if}|$, we have been able to make b/c-type assignments for the ${}^rQ_{K_a}$ transitions with $K_a \leq 6$ and $J = 8$ (Table 1). We determine $I^{(b)}(f \leftarrow i)$ $[I^{(c)}(f \leftarrow i)]$ by adding the intensities of the b-type [c-type] transitions found in the given branch and compute $I^{(b)}(f \leftarrow i)/I^{(c)}(f \leftarrow i)$. The resulting values are included in Table 1 for each ${}^rQ_{K_a}$ -branch. For the branches ${}^rQ_3$, ${}^rQ_4$, ${}^rQ_5$, and ${}^rQ_6$, very small values of $I^{(b)}(f \leftarrow i)/I^{(c)}(f \leftarrow i)$ ensue. The ratio drops from 0.007 for $K_a = 3$ to 0.003 for $K_a = 4$ and further to a minimum of 1.2×10^{-6} at $K_a = 5$. For $K_a = 6$ it increases again to a value of 0.009. The value of 0.007 obtained theoretically for the $J = 8$ transitions in the ${}^rQ_3$ branch is in agreement with the experimental determination[12] of $I^{(b)}(f \leftarrow i)/I^{(c)}(f \leftarrow i) < 0.02$.

Closer inspection of the T_b^{if} and T_c^{if} values in Table 1 allows us to make two observations: (i) b/c-type assignments become ambiguous for $K_a \geq 3$ since for many transitions in the corresponding ${}^rQ_{K_a}$ branches, $|T_b^{if}| \approx |T_c^{if}|$, and (ii) we have already discussed in connection with eqn (24) that in the limit of $K_a \rightarrow \infty$, the line strengths $S_{A'(1)\leftrightarrow A'(2)}$ and $S_{A'(2)\leftrightarrow A'(1)}$ vanish. This is borne out by the TROVE results in Table 1 where we recognize that for these very weak transitions, $T_b^{if} \approx -T_c^{if}$. That is, b-type and c-type contributions to the line strength cancel. This initially unexpected behaviour of the b/c-type intensity ratio was first noted experimentally for the ${}^rQ_3$ branch of HSOH[12] in that $I^{(b)}(f \leftarrow i)/I^{(c)}(f \leftarrow i)$ was determined to be less than 0.02, and it has been satisfactorily explained by theory in the present work (see Fig. 3). That is, the limit of $K_a \rightarrow \infty$ (which, for HSOH, in practice means $K_a \geq 3$) we find transitions for which the b-type and c-type intensity contributions cancel according to eqn (24). We also find 'hybrid' transitions for which the two contributions interfere constructively as described by eqn (23). As already noted, for hybrid transitions b/c-type assignments are meaningless. The ${}^rQ_3$-display in Fig. 4 shows examples of allowed hybrid transitions.

In deriving eqn (15) and (16) we have assumed that the vibrational matrix elements $\left\langle \phi^{(vib)}_{K_a,\tau_{tor}} | \bar{\mu}_b | \phi^{(vib)}_{K'_a,\tau_{tor}} \right\rangle$ and $\left\langle \phi^{(vib)}_{K_a,\tau_{tor}} | \bar{\mu}_c | \phi^{(vib)}_{K'_a,\tau'_{tor}} \right\rangle$, which occur in these equations for $K'_a = K_a + 1$, are independent of τ_{tor} and τ'_{tor}. This condition is relatively well satisfied in the actual TROVE calculations. If we are to describe accurately the intensities of the HSOH transitions, however, it is not permissible to approximate these matrix elements by the values of the dipole moment components at equilibrium, $\bar{\mu}_b{}^e$ and $\bar{\mu}_c{}^e$. The actual values for $\left\langle \phi^{(vib)}_{K_a,\tau_{tor}} | \bar{\mu}_b | \phi^{(vib)}_{K'_a,\tau_{tor}} \right\rangle$ and $\left\langle \phi^{(vib)}_{K_a,\tau_{tor}} | \bar{\mu}_c | \phi^{(vib)}_{K'_a,\tau'_{tor}} \right\rangle$ obtained by

TROVE differ substantially from $\bar{\mu}_b^e$ and $\bar{\mu}_c^e$. Thus, we must calculate the matrix elements numerically and, in particular, take into account the dependence of these matrix elements on K_a and K_a' which arises from the dependence of the torsional wavefunctions $\phi^{(\mathrm{vib})}_{K_a,\tau_{\mathrm{tor}}}$ on K_a. This is illustrated in Fig. 6 where we show the torsional wavefunctions $\phi^{(\mathrm{vib})}_{K_a,\tau_{\mathrm{tor}}=0}$ computed for $K_a = 2$ and $K_a = 8$, as a function of τ_{HSOH}, the dihedral angle between the HSO and SOH planes.[16] We also include in Fig. 6 the two dipole moment components $\bar{\mu}_b(\tau_{\mathrm{HSOH}})$ and $\bar{\mu}_c(\tau_{\mathrm{HSOH}})$, calculated along the torsional MEP of HSOH.[15] The wavefunction $\phi^{(\mathrm{vib})}_{K_a=2,\tau=0}(\tau_{\mathrm{HSOH}})$ has its maximum amplitude near the equilibrium τ_{HSOH}-value, $\tau_{\mathrm{eq}} = 91.4°$, whereas the maximum amplitude of $\phi^{(\mathrm{vib})}_{K_a=8,\tau=0}(\tau_{\mathrm{HSOH}})$ occurs at $\tau_{\mathrm{HSOH}} = 126.3°$. That is, relative to $\phi^{(\mathrm{vib})}_{K_a=2,\tau=0}(\tau_{\mathrm{HSOH}})$, the wavefunction $\phi^{(\mathrm{vib})}_{K_a=8,\tau=0}(\tau_{\mathrm{HSOH}})$ has its maximum amplitude shifted towards the *trans*-planar configuration at $\tau_{\mathrm{HSOH}} = 180°$. The quantum number K_a is the projection, in units of $\hbar$, of the total angular momentum onto the molecule-fixed a axis which almost coincides with the SO bond in HSOH. That is, K_a measures how the entire molecule rotates about the SO bond which is also the axis that defines the torsional motion. Because of this, there is a strong coupling between the torsion and the K_a-type rotation and this coupling manifests itself in the wavefunctions included in Fig. 6: When the molecule rotates faster, centrifugal effects cause the dihedral angle τ_{HSOH} to open. The shift of the maximum amplitude of the wavefunctions towards $\tau_{\mathrm{HSOH}} = 180°$ causes the matrix elements $\left\langle \phi^{(\mathrm{vib})}_{K_a,\tau_{\mathrm{tor}}} | \bar{\mu}_b | \phi^{(\mathrm{vib})}_{K_a'\tau_{\mathrm{tor}}} \right\rangle$ and $\left\langle \phi^{(\mathrm{vib})}_{K_a,\tau_{\mathrm{tor}}} | \bar{\mu}_c | \phi^{(\mathrm{vib})}_{K_a'\tau_{\mathrm{tor}}'} \right\rangle$ to decrease, since the dipole moment components $\bar{\mu}_b(\tau_{\mathrm{HSOH}})$ and $\bar{\mu}_b(\tau_{\mathrm{HSOH}})$ both decrease when τ_{HSOH} approaches 180°. Thus the strong variation of $\bar{\mu}_b(\tau_{\mathrm{HSOH}})$ and $\bar{\mu}_c(\tau_{\mathrm{HSOH}})$ with τ_{HSOH}, and the strong dependence of the wavefunctions $\left| \phi^{(\mathrm{vib})}_{K_a,\tau_{\mathrm{tor}}} \right\rangle$ on K_a, both lead to a strong dependence of T_b^{if} and T_c^{if} on K_a (see Table 1), and to a strong variation of the ratio I_b/I_c with K_a.

Along with the rotational spectrum of HSOH shown in Fig. 1, we have also simulated the rotational spectrum

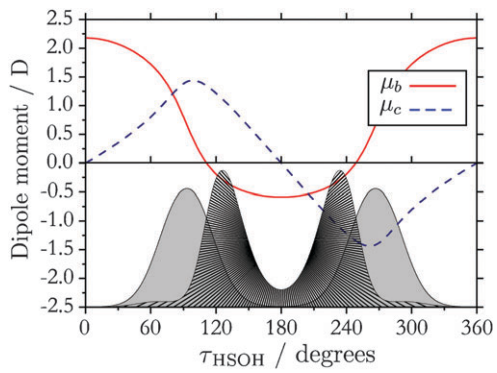

Fig. 6 Upper part: The two dipole moment components $\bar{\mu}_b(\tau_{\mathrm{HSOH}})$ (solid curve) and $\bar{\mu}_c(\tau_{\mathrm{HSOH}})$ (dashed curve), calculated along the torsional MEP of HSOH shown in Fig. 1 of ref. 15. Lower part: The torsional wavefunctions $\phi^{(\mathrm{vib})}_{K_a=2,\tau_{\mathrm{tor}}=0}(\tau_{\mathrm{HSOH}})$ (area under curve uniformly semi-transparent grey) and $\phi^{(\mathrm{vib})}_{K_a=8,\tau_{\mathrm{tor}}=0}(\tau_{\mathrm{HSOH}})$ (area under curve inhomogeneously shaded) for HSOH, drawn in arbitrary units. All functions in the figure depend on τ_{HSOH}, the dihedral angle between the HSO and SOH planes.[16]

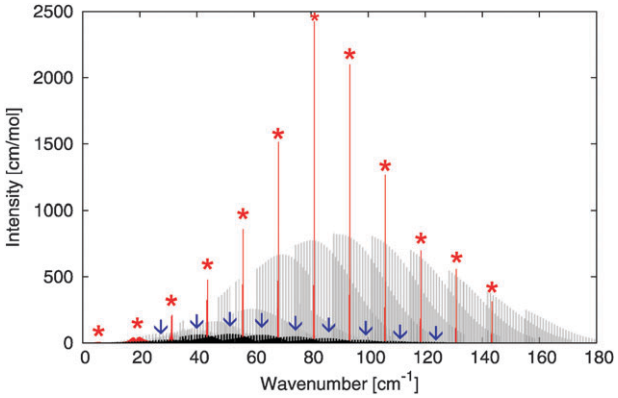

Fig. 7 The rotational spectrum of HSOH associated with the fundamental torsional state at 440 cm^{-1}, simulated theoretically at $T = 300$ K. ^rP- and ^rQ-branch transitions are indicated by arrows and asterisks, respectively.

associated with the first excited torsional state ν_{HSOH} located at 440 cm^{-1}. The transitions in this spectrum all originate and end in the ν_{HSOH} fundamental state. The RPH/SRB approach[25–27] used for the nuclear-motion calculations of the present work is also valid for the ν_{HSOH} state which is well below the lowest small-amplitude vibrational state, the SO stretch fundamental state near 760 cm^{-1} (see ref. 16). In fact even higher torsionally excited states are well described by the RPH/SRB approach, see ref. 15. The simulated ν_{HSOH}-state rotational spectrum ($T = 300$ K, $J \leq 40$) is shown in Fig. 7. The 'hot' spectrum is very similar to the ground-state rotational spectrum of Fig. 1, but the intensities are reduced by a factor of four.

We have also analyzed the calculated torsional splittings Δ_{tor} ($\nu_{\mathrm{HSOH}} = 1, J, K_a, \tau_{\mathrm{rot}}$) associated with the ν_{HSOH} state. In Fig. 8 we plot for each K_a-value the splittings calculated for $J = K_a, \ldots, 40$. We find that the main pattern of the ground state splittings[15] are reproduced here: the irregular K_a-variation of the splittings for the lowest K_a-values and the period-of-three variation as K_a increases.[15] Relative to the ground state, the splittings in Fig. 8 are larger by two orders of magnitude.

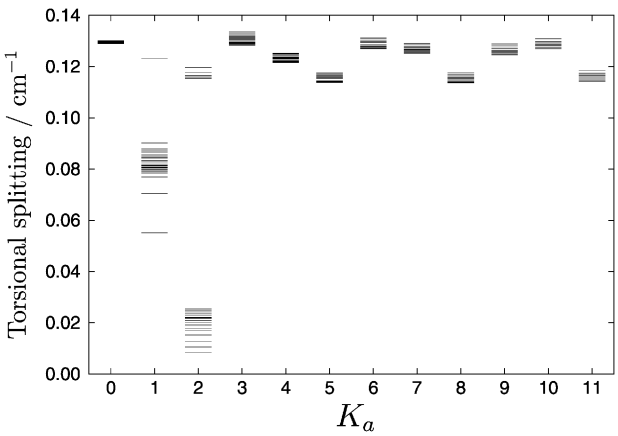

Fig. 8 The theoretical values of the torsional splittings Δ_{tor} ($\nu_{\mathrm{HSOH}} = 1, J, K_a, \tau_{\mathrm{rot}}$) (in cm^{-1}), plotted against the rotational quantum number K_a. For each K_a-value, we plot splittings calculated for $J = K_a, \ldots, 40$ and $\tau_{\mathrm{rot}} = 0$ and 1.

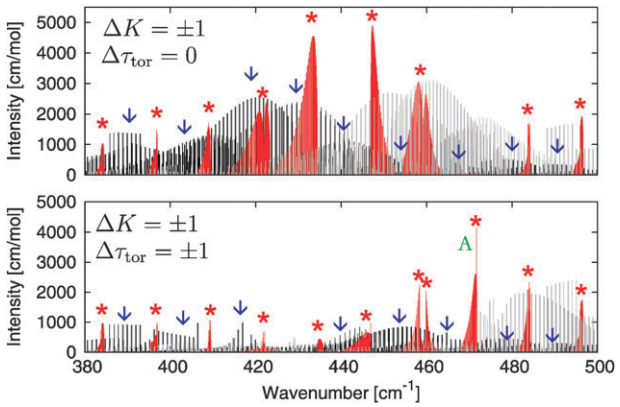

Fig. 9 The fundamental torsional band of HSOH, simulated theoretically at $T = 300$ K. The transitions are separated into a $\Delta\tau_{tor} = 0$ spectrum in the upper display and a $\Delta\tau_{tor} = \pm 1$ spectrum in the lower display (see text). The *P*- and *Q*-branch transitions are indicated by arrows and asterisks, respectively.

Finally, we report the simulation of the ν_{HSOH} fundamental band of HSOH (Fig. 9). The calculations are done for $T = 300$ K, taking into account transitions between states with $J \leq 40$. Only transitions with $\Delta K_a = \pm 1$ are plotted in Fig. 9 since the $K_a = 0$ transitions are vanishingly weak in comparison with the $K_a = \pm 1$ ones. We separate the spectrum into a $\Delta\tau_{tor} = 0$ spectrum (which, in the case of separable rotation–torsion wavefunctions, consists of *b*-type transitions) and a $\Delta\tau_{tor} = \pm 1$ spectrum (which, in the case of separable rotation–torsion wavefunctions, consists of *c*-type transitions). For the assignment of the transitions in the Figure, we used an automatic procedure which assigns to a given state the K_a and τ_{tor} values of the basis function with the largest contribution to the state, *i.e.* the basis function with the largest absolute value of the expansion coefficients in eqn (3). Because of the strong torsion–rotation interaction (see discussion above) this approach occasionally leads to 'unsystematic' assignments. As an example of this, it is surprising that all transitions in the sub-band marked 'A' in the lower display of Fig. 9 are assigned as belonging to the $\Delta\tau_{tor} = \pm 1$ spectrum. Clearly this sub-band, or at least some of the transitions in it, could reasonably be assigned as belonging to the $\Delta\tau_{tor} = 0$ spectrum (top display).

IV. Summary and discussion

The program suite TROVE[24] for calculating the rotation–vibration energies of an arbitrary molecule in an isolated electronic state has recently been extended[32] by modules to compute the intensities of rotation–vibration transitions such that rotation–vibration spectra can be simulated. The present simulations of the rotation–torsion spectrum of $H^{32}SOH$ are based on *ab initio* potential energy and dipole moment surfaces for the electronic ground state of HSOH, calculated at the CCSD(T) level of theory using the aug-cc-pV(T+*d*)Z and aug-cc-pV(Q+*d*)Z basis sets.[20–23]

The current work is mainly motivated by the recent experimental observation of intensity anomalies in some of the ${}^rQ_{K_a}$-branches of the HSOH rotational spectrum recorded at 1.3 THz with a synthesizer-based multiplier spectrometer.[12] An experimentally observed ${}^rQ_{K_a}$-branch in the HSOH spectrum is customarily assigned in a pattern-recognition process which attempts to separate the transitions of the ${}^rQ_{K_a}$-branch into two sets of *b*-type and *c*-type transitions. The dipole moment of HSOH is approximately perpendicular to the SO bond which almost coincides with the *a* principal axis. Consequently, the dipole moment component $\bar{\mu}_a$ along the *a* axis is small whereas the *b* and *c* components, $\bar{\mu}_b$ and $\bar{\mu}_c$, are comparatively large. Conventional spectroscopic wisdom assumes that a *b*-type (*c*-type) transition predominantly derives its intensity from $\bar{\mu}_b$ ($\bar{\mu}_c$), and that the ratio of typical *b*-type and *c*-type transition intensities, I_b/I_c, is roughly given by eqn (7) which predicts $I_b/I_c \approx 0.3$ for HSOH.

Experimentally[12] it has been found that transitions of the ${}^rQ_0$ and ${}^rQ_1$ branches of HSOH can be straightforwardly separated into *b*-type and *c*-type transitions with a value of $I_b/I_c \approx 0.3$. That is, these two branches behave according to the conventional spectroscopic wisdom. The transitions of the ${}^rQ_2$ branch of HSOH can also be assigned as *b*-type or *c*-type but here $I_b/I_c \approx 0.6$, twice as large as the value predicted by eqn (7). In contrast, for the ${}^rQ_3$ branch the *b*-type transitions are very weak compared to the *c*-type ones and experiment yields $I_b/I_c < 0.02$.

The present theoretical calculations produce intensity values for the ${}^rQ_{K_a}$-branch transitions in perfect agreement with the experimental findings (see Table 1). Our analysis of the theoretical results (Section III) shows that eqn (7) applies when the rotation–torsion wavefunctions for the states involved in the transitions, $\Psi^{\Gamma,i)}_{J,K_a,i}$, are separable as $\Psi^{\Gamma,i)}_{J,K_a,i} \approx |J, K_a, \tau_{rot}\rangle \phi^{(vib)}_{K_a,\tau_{tor}}$ As mentioned in connection with eqn (1), the parity[28] of the rotational basis function $|J,K_a,\tau_{rot}\rangle$ is $(-1)^{\tau_{rot}}$, and the parity of the torsional basis function $\phi^{(vib)}_{K_a,\tau_{tor}}$ is $(-1)^{\tau_{tor}}$. We have shown in section III [see, in particular, eqn (15) and (16)], that for HSOH, separable wavefunctions [*i.e.*, $\theta_{J,K_a} \approx 0$ in eqn (8)–(11)] are obtained for $K_a = 0$, 1, and 2. This explains the experimental result[12] that eqn (7) is well satisfied for the ${}^rQ_0$ and ${}^rQ_1$ branches of HSOH.

As K_a increases, HSOH approaches the so-called symmetric top limit. In this limit, $\theta_{J,K_a} \approx 45°$ in eqn (8)–(11) and the rotation–torsion wavefunctions $\Psi^{\Gamma,i)}_{J,K_a,i}$ become fifty–fifty mixtures of products $|J, K_a, \tau_{rot}\rangle \phi^{(vib)}_{K_a,\tau_{tor}}$ with a common value of $(\tau_{rot} + \tau_{tor})$ mod 2 (=0 or 1). With $\theta_{J,K_a} \approx 45°$ in eqn (8)–(11), the intensities of the ${}^rQ_{K_a}$ transitions are given by eqn (23) and (24) which, at least formally, are consistent with $I_b/I_c = 0$, in keeping with the experimental result[12] of $I_b/I_c < 0.02$ for the ${}^rQ_3$ branch of HSOH.

The ${}^rQ_2$ branch of HSOH is neither described by the limiting case $\theta_{J,K_a} \approx 0$ nor by the other limiting case, the symmetric top limit with $\theta_{J,K_a} \approx 45°$. The TROVE calculations give a theoretical value of $I_b/I_c = 0.6$ for this branch (Table 1), in perfect agreement with the experimental value[12] of 0.58. Hence they also remain reliable in the intermediate range between the low-K_a and high-K_a limits. Closer inspection of the TROVE results indicates that the expected limiting behaviour of a symmetric top is not fully reached with increasing K_a, since the computed I_b/I_c values do not vanish completely as implied by eqn (24). These ratios drop from

0.007 for $K_a = 3$ to 0.004 for $K_a = 4$ and further to a minimum of 2.5×10^{-6} at $K_a = 5$, but increase again to 0.009 for $K_a = 6$. Such deviations from the symmetric-top limit are not too surprising since the underlying qualitative model neglects a number of factors that are taken into account in the actual TROVE calculations, including the actual degree of wavefunction mixing (with θ_{J,K_a} somewhat different from 45°) as well the vibrational dependence of the dipole moment components and the variation of the vibrational dipole-moment matrix elements with K_a and K_a'.

In summary, the present study demonstrates that the variational TROVE approach provides a realistic description of the large amplitude torsional motion of HSOH. The simulations provide rotation–torsion spectra of HSOH that reproduce the observed intensity patterns very well, including the intensity anomalies in the ${}^rQ_{K_a}$-branches which are caused by the large-amplitude torsional motion; these anomalies can be understood qualitatively by an analysis of the TROVE results.

Appendix A: The line strength

The line strength $S(f \leftarrow i)$ of an individual rovibrational transition $f \leftarrow i$ is used in eqn (4). It is initially expressed in terms of the matrix elements of the dipole moment function between the rotation–torsion wavefunctions in eqn (3). For the calculations of the present work, we use

$$S(f \leftarrow i) = g_{\rm ns}(2J'+1)(2J''+1) \times \left| \sum_{v'_{\rm HSOH},K',\tau'_{\rm rot}} \sum_{v''_{\rm HSOH},K'',\tau''_{\rm rot}} (-1)^{\sigma'_{\rm rot}+\sigma''_{\rm rot}+K''} \times C_{J,\Gamma',f}^{(K',\tau'_{\rm rot},v'_{\rm HSOH},\tau'_{\rm tor})} C_{J,\Gamma'',i}^{(K'',\tau''_{\rm rot},v''_{\rm HSOH},\tau''_{\rm tor})} \times \begin{pmatrix} J'' & 1 & J' \\ K'' & K''-K' & -K' \end{pmatrix} F_{v',K',\tau'_{\rm rot};v'',K'',\tau''_{\rm rot}} \right|^2, \quad \text{(A1)}$$

where the quantum numbers

$$(J', K', \tau'_{\rm rot}, \tau'_{\rm tor}, v'_{\rm HSOH}, \sigma'_{\rm rot})$$

apply to the final state of the transition and

$$(J'', K'', \tau''_{\rm rot}, \tau''_{\rm tor}, v''_{\rm HSOH}, \sigma''_{\rm rot})$$

to the initial state. The expansion coefficients $C_{J,\Gamma',f}^{(K',\tau'_{\rm rot},v'_{\rm HSOH},\tau'_{\rm tor})}$ and $C_{J,\Gamma'',i}^{(K'',\tau''_{\rm rot},v''_{\rm HSOH},\tau''_{\rm tor})}$ are defined in eqn (3). Furthermore,

$$F_{v',K',\tau'_{\rm rot};v'',K'',\tau''_{\rm rot}} = \begin{cases} (\tau''_{\rm rot}-\tau'_{\rm rot})\langle v'|\bar{\mu}_z|v''\rangle, & K'=K'', \tau'_{\rm rot}\neq\tau''_{\rm rot} \\ f_{K',K''}(\tau'_{\rm rot}-\tau''_{\rm rot})(K''-K')\langle v'|\bar{\mu}_x|v''\rangle, & K''-K'|=1, \tau'_{\rm rot}\neq\tau''_{\rm rot} \\ -f_{K',K''}\langle v'|\bar{\mu}_y|v''\rangle, & |K''-K'|=1, \tau'_{\rm rot}=\tau''_{\rm rot} \end{cases} . \quad \text{(A2)}$$

These expressions have been derived by following the procedure described in Chapter 14 of ref. 28 and in ref. 30. They are given in terms of the symmetrized rotational basis functions in eqn (73) and (74) of ref. 24. In eqn (A2), $\begin{pmatrix} J'' & 1 & J' \\ K'' & K''-K' & -K' \end{pmatrix}$ is a standard 3*j*-symbol (see, for example) ref. 28,

$$f_{K',K''} = \begin{cases} \frac{1}{\sqrt{2}} & \text{for } K'+K''\neq 1 \\ 1 & \text{otherwise} \end{cases} \quad \text{(A3)}$$

$$\sigma_{\rm rot} = \begin{cases} K \bmod 3 & \text{for } \tau_{\rm rot}=1 \\ 0 & \text{otherwise,} \end{cases} \quad \text{(A4)}$$

and

$$|v\rangle = |v_{\rm OS}\rangle\,|v_{\rm SH}\rangle\,|v_{\rm OH}\rangle\,|v_{\rm OSH}\rangle\,|v_{\rm SOH}\rangle\,|v_{\rm HSOH},\tau_{\rm tor}\rangle \quad \text{(A5)}$$

is a vibrational basis function as introduced in eqn (1). In eqn (A1) and (A2) $\bar{\mu}_\alpha$ ($\alpha = a, b, c$) are electronically averaged dipole moment components $\langle\Phi_{\rm elec}|\mu_\alpha|\Phi_{\rm elec}\rangle$ expressed in the molecule-fixed axis system *xyz* defined by Eckart–Sayvetz conditions.[24]

Acknowledgements

We acknowledge support from the European Commission (contract no. MRTN-CT-2004-512202 "Quantitative Spectroscopy for Atmospheric and Astrophysical Research" (QUASAAR)).

References

1 R. J. Huxtable, *Biochemistry of Sulphur*, Plenum Press, New York, 1986.
2 C. F. Cullis and M. M. Hirschler, *Atmos. Environ.*, 1980, **14**, 1263–1278.
3 N. S. Wang and C. J. Howard, *J. Phys. Chem.*, 1990, **94**, 8787–8794.
4 G. S. Tyndal and A. R. Ravishankara, *Int. J. Chem. Kinet.*, 1991, **23**, 483–527.
5 L. Vervisch, B. Labegorre and J. Réveillon, *Fuel*, 2004, **83**, 605–614.
6 G. Winnewisser, F. Lewen, S. Thorwirth, M. Behnke, J. Hahn, J. Gauss and E. Herbst, *Chem.–Eur. J.*, 2003, **9**, 5501–5510.
7 M. Behnke, J. Suhr, S. Thorwirth, F. Lewen, H. Lichau, J. Hahn, J. Gauss, K. M. T. Yamada and G. Winnewisser, *J. Mol. Spectrosc.*, 2003, **221**, 121–126.
8 S. Brünken, M. Behnke, S. Thorwirth, K. M. T. Yamada, T. F. Giesen, F. Lewen, J. Hahn and G. Winnewisser, *J. Mol. Struct.*, 2005, **742**, 237–242.
9 O. Baum, S. Esser, N. Gierse, S. Brünken, F. Lewen, J. Hahn, J. Gauss, S. Schlemmer and T. F. Giesen, *J. Mol. Struct.*, 2006, **795**, 256–262.
10 H. Beckers, S. Esser, T. Metzroth, M. Behnke, H. Willner, J. Gauss and J. Hahn, *Chem.–Eur. J.*, 2006, **12**, 832–844.
11 O. Baum, T. F. Giesen and S. Schlemmer, *J. Mol. Spectrosc.*, 2008, **247**, 25–29.
12 O. Baum, M. Koerber, O. Ricken, G. Winnewisser, S. N. Yurchenko, S. Schlemmer, K. M. T. Yamada and T. F. Giesen, *J. Chem. Phys.*, 2008, **129**, 224312.
13 O. Baum, *PhD dissertation*, University of Cologne, 2008.
14 K. M. T. Yamada, G. Winnewisser and P. Jensen, *J. Mol. Struct.*, 2004, **695–696**, 323–337.
15 R. I. Ovsyannikov, V. V. Melnikov, W. Thiel, P. Jensen, O. Baum, T. F. Giesen and S. N. Yurchenko, *J. Chem. Phys.*, 2008, **129**, 154314.

16 S. N. Yurchenko, A. Yachmenev, W. Thiel, O. Baum, T. F. Giesen, V. V. Melnikov and P. Jensen, *J. Mol. Spectrosc.*, 2009, **257**, 57–65.
17 K. M. T. Yamada, P. Jensen, S. C. Ross, O. Baum, T. F. Giesen and S. Schlemmer, *J. Mol. Struct.*, 2009, **927**, 96–100.
18 G. D. Purvis and R. J. Bartlett, *J. Chem. Phys.*, 1982, **76**, 1910–1918.
19 K. Raghavachari, G. W. Trucks, J. A. Pople and M. Head-Gordon, *Chem. Phys. Lett.*, 1989, **157**, 479–483.
20 T. H. Dunning, *J. Chem. Phys.*, 1989, **90**, 1007–1023.
21 R. A. Kendall, T. H. Dunning and R. J. Harrison, *J. Chem. Phys.*, 1992, **96**, 6796–6806.
22 D. E. Woon and T. H. Dunning, *J. Chem. Phys.*, 1993, **98**, 1358–1371.
23 A. K. Wilson and T. H. Dunning, *J. Chem. Phys.*, 2003, **119**, 11712–11714.
24 S. N. Yurchenko, W. Thiel and P. Jensen, *J. Mol. Spectrosc.*, 2007, **245**, 126–140.
25 W. H. Miller, N. C. Handy and J. A. Adams, *J. Chem. Phys.*, 1980, **72**, 99–112.
26 J. T. Hougen, P. R. Bunker and J. W. C. Johns, *J. Mol. Spectrosc.*, 1970, **34**, 136–172.
27 P. R. Bunker and B. M. Landsberg, *J. Mol. Spectrosc.*, 1977, **67**, 374–385.
28 P. R. Bunker and P. Jensen, *Molecular Symmetry and Spectroscopy*, NRC Research Press, Ottawa, 2nd edn, 1998.
29 J. W. Cooley, *Math. Comput.*, 1961, **15**, 363–374.
30 S. N. Yurchenko, M. Carvajal, W. Thiel, H. Lin and P. Jensen, *Adv. Quantum Chem.*, 2005, **48**, 209–238.
31 S. N. Yurchenko, M. Carvajal, P. Jensen, H. Lin, J. J. Zheng and W. Thiel, *Mol. Phys.*, 2005, **103**, 359–378.
32 S. N. Yurchenko, R. J. Barber, A. Yachmenev, W. Thiel, P. Jensen and J. Tennyson, *J. Phys. Chem. A*, 2009, **113**, 11845–11855.
33 E. A. Desloge, *Am. J. Phys.*, 1984, **52**, 261–262.
34 D. Papoušek and M. R. Aliev, *Molecular Vibrational/Rotational Spectra*, Elsevier, Amsterdam, 1982.
35 G. Winnewisser, *Vib. Spectrosc.*, 1995, **8**, 241–253.
36 G. Winnewisser and K. M. T. Yamada, *Vib. Spectrosc.*, 1991, **1**, 263–272.
37 G. Pelz, K. M. T. Yamada and G. Winnewisser, *J. Mol. Spectrosc.*, 1993, **159**, 507–520.
38 P. R. Bunker and P. Jensen, *Fundamentals of Molecular Symmetry*, IOP Publishing, Bristol, 2004.